Journal of Computational Applied Mechanics 2024, 55(-): PP-PP

DOI: 10.22059/JCAMECH.2024.373641.995

RESEARCH PAPER

Analyzing the Buckling Behavior of In-plane Bidirectional Functionally Graded Porous Plates

Bathini Sidda Reddy [a*], K. Vijaya Kumar Reddy [b]

[a] *Department of Mechanical Engineering, Rajeev Gandhi Memorial College of Engineering and Technology, Nandyal-518501, A.P, India*

[b] *Department of Mechanical Engineering, Jawaharlal Nehru Technological University, Hyderabad, India*

Abstract

The spacecraft and space shuttles demand novel engineering materials to meet the required properties. This can be accomplished by altering the material properties in more than one direction. The introduction of inplane bidirectional functionally graded materials with porosity are expected to exhibit these properties. This paper presents the buckling analses of inplane bidirectional (2-D) functionally graded porous plates (IBFGPPs) considering uniform porosity distribution in uni-axial and bi-axial compression. The effective modulus of elasticity of the material is varied in in x-and y-axes by employing the rule of mixtures. The higherorder theory used for the study of buckling response meets the nullity requirements at plate's upper and lower surface and derived the equations of motion thru Lagrange equations. The displacement functions are formulated in simple algebraic polynomials, incorporating admissible functions to satisfy the simply supported conditions in both axial and transverse directions. The components of admissible functions are derived by Pascal's triangle. Accurateness of this theory is judged by comparing it to existing numerical data in the literature. The effect of thickness ratio's (a/h), aspect ratio's (b/a), exponents ($\zeta_1$and ζ_2) in η_1 and η_2-direction, and the porosity on the buckling response of IBFGPPs are examined comprehensively. The numerical findings provided here serve as reference solutions for evaluating diverse plate theories and for comparing them against results obtained through alternative analytical and finite element techniques. From the obtained results, it can be inferred that the proposed theory facilitates the assessing of buckling tendencies of in-plane bi-directional porous FG plates produced through sintering process and could be deemed as a pivotal in the process of optimizing he design of the IBFGPPs.

Keywords: Inplane bidirectional FGP's; Buckling analyses;Rule of Mixtures;Lagrange Equations;Porosity coefficient;

1. Introduction

Functionally graded materials (FGMs) are novel materials, first found by researchers from Japan in the mid-1980s [1]. These are engineered with at least two dissimilar constituents and alter the material properties continuously in spatial directions to attain specific properties that are markedly differ from those of its individual constituents. Thus,

* Corresponding author. Tel.: +91 9440844600; fax: 08514275203.
E-mail address: bathinisiddareddy@rgmcet.edu.in

reduces the failures caused by stress and strain discontinuities at the interface. Furthermore, porosity improves the stiffness and decreases structure's density. Therefore, porous materials have found extensive use in numerous engineering domains such as aerospace, space exploration, and defense applications. Hence, by the fusion of the FGMs with porous materials, results in the creation of a unique material termed "porous FGMs" [2, 3]. Novel materials of this nature are developed by manipulating the pore coefficient and the microstructure of the materials.

Moreover, the usage of a combination of materials is on the rise, because traditional engineering materials fall short of meeting the required characteristics by the various industries. Plates serve as fundamental elements extensively employed across various structures, including but not limited to aircraft and space vehicles to automotive, ship-building, civil engineering, energy production, the chemical industry, optical systems, biomedical applications, and mechanical engineering [4, 5].

Buckling in IBFGPPs holds significant importance in structural engineering and materials science. These plates, which possess varying material properties through their thickness and in two orthogonal directions, are increasingly employed in aerospace, automotive, and civil engineering applications. If the applied inplane loads exceeds critical buckling load in these applications, the structure results in instability. Understanding their buckling behavior is critical for optimizing their structural performance and preventing catastrophic failures. By comprehending the buckling characteristics of these plates, engineers can design lightweight and resilient structures that make efficient use of advanced materials, ultimately enhancing safety, performance, and cost-effectiveness in various industries.

Therefore, it is important to examine the buckling analyses of FGPs under both uniaxial and biaxial compressive loads. In the past, many researchers investigated the buckling behavior of unidirectional FGPs. Mohammadi et al. [6, 7] studied the buckling response of thin and reasonably thick unidirectional FG rectangular plates. The material properties were varied in the thickness. Farajpour et al. [8-10], analyzed the buckling of nanoplates by utilising nonlocal continuum mechanics. They considered the variable thickness in rectangular plates, circular graphene sheets and micro/nanoscale plates subjected to linearly in-plane load that vary linearly. The shear buckling analysis of orthotropic graphene sheets with a single layer has been investigated by Mohammadi et al [11] under a temperature environment by utilising nonlocal elasticity theory. Abdollahi et al. [12] analyzed thick FG rectangular piezoelectric plates for buckling by higher order plate theory.

Mohammadi and Mahani [13] analyzed the buckling response of rectangular microplates by means of the sizedependent Kirchhoff plate model. Modified version of strain gradient theory and modified version of couple stress theory was adopted to obtain the critical buckling loads. Also investigated the effect of dimensions, length-scale parameters and loading condition states on the buckling loads. Moreover Farajpour et al. [14] developed a sizedependent plate model using higher-order non-local strain-gradient theory to investigate the buckling behaviour of three distinct types of graphene sheets in varying aspect ratios, different scale parameters composed with elastic medium coefficients, change in temperature and change in the nanoplate length. Farajpour et al. [15] used piezoelectric nanoshell to investigate the dynamics of microtubules (MTs) within an elastic medium subjected to thermal conditions encompassing vibration, buckling, and smart control. It delved into the effect of different factors, including elastic properties of the surrounding medium, characteristics of the internal filament matrix, scaling coefficient, applied electric voltage, the ratio of radius to thickness in a piezoelectric nanoshell, and temperature variations on the smart control of MTs.

Buckling behavior of unidirectional FGPs was examined by Sidda Reddy et al. [16, 17] using higher order theory. The influence of thickness ratio, aspect ratio and also modulus ratio on the critical buckling load was investigated. Kim et al. [5, 18] reported numerical findings regarding the static characteristics of functionally graded micro plates including porosity. The plate analysis theories employed did not meet the nullity requirements. Furthermore, the study examined the impact of porosity, exponent index, and material length-scale factor on these properties.

Vinh et al. [19] analysed the static bending and buckling analyses of bidirectional FGPs with porosity using improved first order theory. Yang et al. [20] conducted a comparative analysis of the bending and buckling behavior exhibited by various types of porous functionally graded plates in comparison to a conventional sandwich plate. The solutions were derived through the application of the Ritz method with Chebyshev polynomials.

The authors in Refs. [6, 20] altered the properties of the materials in only one particular direction which may not provide desirable properties for components utilized in propulsion systems and space related applications. These applications frequently experience significant temperature variations in multiple directions [21]. To achieve this objective, 2-D FGMs are introduced, playing a significant role in the design and advancement of cutting-edge engineering applications, such as space crafts and space shuttles. These applications demand highly effective high-temperature-resistant materials. Consequently, the development of 2-D or multidirectional FGMs becomes indispensable and valuable while designing the advanced structures. In light of this, the literature provides a brief overview of bi-directional FGMs e.g., see [21, 22].

Nemat-Alla [21], introduced two-directional Functionally Graded Materials (FGMs), demonstrating through numerical analysis that they exhibit superior capabilities in lowering temperature stresses when compared to 1-D

FGMs. Recent research efforts have delved into the realm of bi-directional FGMs, with notable contributions in the open source. For instance, Nemat-Alla [23] enhanced material compositions, employing finite element models to mitigate temperature-induced stresses in 2-D FGMs subjected to severe temperature condition cycles featuring ZrO2 / 6061 - T6 / Ti – 6 Al - 4V materials.

vibrational analyses of bidirectional Functionally Graded thick hollow cylinders were explored by formulating 3-D elasticity equations [24] and differential and integral quadrature methods [25].

Numerous research endeavors have been undertaken concerning 2-D FG Euler-Bernoulli/Timoshenko beams, nanobeams, and their nonlinear bending [26], vibrational characteristics [27, 28], and buckling analyses [29, 30], to name just a few examples.

Karamanli [31] employed a quasi-3dimensional shear deformation theory to investigate the bending of 2-D Functionally Graded sandwich beams, whereas LezgyNazargah [32] utilized NURBS based isogeometric analyses to examine the thermomechanical properties of 2-Dimensional FG beams. In line with the observations of Apalak and Demirbas [33], gradient exponents may not significantly impact temperature distributions but notably influence heat transfer durations in bidirectional FGMs.

The bending and buckling behavior of 2-D FGP structures were investigated by Van Do et al. [34] using third order plate theory and finite element methods. Their findings revealed that obtaining results for bi-directional FGPs is more intricate than unidirectional counterparts due to the material gradation in two distinct directions. The bending and free vibration characteristics of in-plane bi-directional FGPs, accounting for variable thickness adopting Iso-geometric analysis were explored by Lieu et al. [35]. Furthermore, Lieu et al. [36] delved into the free vibration and buckling analyses of in-plane bidirectional FGPs, employing nonuniform rational Bspline based material mesh and generalized shear deformation plate theory.

Chen et al. [37] combined the first-order plate theory with isogeometric analysis to examine the natural frequency of sector cylindrical shells crafted from 2-D FGMs by restrained edges. Esmaeilzadeh and Kadkhodayan [38] tackled dynamic analysis of 2-D FGPs reinforced by eccentrically positioned outside stiffeners with moving loads at a constant velocity.

Abbas Barati et al. [39] explored various aspects of bi-directional functionally graded nanobeams under a longitudinal magnetic field, incorporating small-scale effects through nonlocal elasticity theory. The impact of general boundary restraints and geometrical imperfections on the vibration of bidirectional functionally graded rectangular plates was investigated by Chen et al. [40].

Additionally, Vinh [22] conducted an extensive study on the static behavior of 2-D FG sandwich plates. This investigation utilized a higher order theory in combination of finite element methods. The study found that the change in material composition, properties, boundary conditions, and layer thickness ratios play significant roles in the structural behavior.

FGMs are fabricated using various techniques. However, in the sintering process used for FGM production, porosities and microvoids may arise due to the differing temperature requirements of the metal and ceramic phases. These pores can significantly compromise material strength [41]. Therefore, it is imperative to judge the impact of porosity in the design of bi-directional FGM components. Sidda Reddy et al. [42] conducted for the free vibration analyses of 2-D FGPs with porosities, employing a refined first order theory.

Reza Kolahchi et al. [43] investigated the nonlinear dynamic stability of temperature-dependent viscoelastic plates reinforced by single-walled carbon nanotubes (SWCNTs) considering both uniform and functionally graded distribution patterns. The viscoelastic properties of the plate are based on Kelvin–Voigt theory, and the surrounding elastic medium is modelled orthotropically. The dynamic buckling optimization of laminated nanocomposite conical aircraft shells in varied environmental conditions, incorporating moisture, temperature, and magnetic fields was explored by Behrooz Keshtegar et al. [44]. This optimization employs an enhanced Grey Wolf optimization (GWO) algorithm, integrating instability and frequency considerations as subjective and objective functions, respectively. Reza Kolahchi et al. [45] investigated the dynamic stability of nanocomposite sandwich truncated conical shells with a graphene platelets (GPLs)-reinforced core and magneto-strictive face sheets. Various parameters including boundary conditions, controller, damping, and GPLs volume percentage were analyzed, and showed that increase of GPLs volume percentage raises the excitation frequency.

Wave propagation and vibration in a porous beam embedded with nanocomposite piezoelectric layers, utilizing various non-uniform graphene nanoplatelet (GPL) reinforcement patterns was investigated in Ref. [46]. In this study, the structure's viscoelastic properties were modeled using a Kelvin-Voigt model with a Kerr viscoelastic foundation. The seismic response of underwater fluid-conveying concrete pipes reinforced with nano-fiber reinforced polymer (NFRP) layers during the Kobe earthquake was investigated by Hadi Golabchi et al. [47] on fluid velocity analysis on the instability of pipes reinforced by silica nanoparticles (SiO2). Their Results indicated that increase in volume fractions of SiO2 nanoparticles, the frequency and critical fluid velocity of the structure were increased. Furthermore, considering SiO2 nanoparticles agglomeration, decreased the frequency and critical fluid velocity of the pipe. The

seismic response of underwater fluid-conveying concrete pipes reinforced with nano-fiber reinforced polymer (NFRP) layers was studied by Reza Kolahchi et al. [48]. The results showing that increase of NFRP layer thickness and volume percentage decreases the dynamic deflection, while factors such as inner and outer fluids and agglomeration of nano fibers increase it, along with increasing length to thickness ratio. Al-Furjan et al. [49] studied the dynamic stability of an Aluminum beam embedded with nanocomposite piezoelectric layers reinforced with Carbon nanotubes (CNTs), considering agglomeration effects via the Mori-Tanaka model. Their findings revealed that a 14 % reduction in instability region due to CNT agglomeration. Reza Kolahchi et al. [50] explored low-velocity impact on nanocomposite sandwich truncated conical shells (NSTCS) with graphene platelets (GPLs)-reinforced core and magneto-strictive face sheets. They employed higher-order shear deformation theory (HSDT) and Kelvin–Voigt model and found that increase of GPLs volume percentage enhances deflection and maximum contact force while reduces contact duration.

A mathematical model was presented for dynamic response of sandwich plates under blast loads using a numerical approach [51]. This study revealed that magnetic field on face sheets and hygro-thermal conditions significantly influenced 24% increase in dynamic displacement. Reza Kolahchi and Farzad Kolahdouzan [52] assessed the dynamic stability of a viscoelastic defective single-layered graphene sheet (SLGS), considering various defects (SV, DV, SW) and their reconstruction effects, under hygrothermal loads and in-plane magnetic forces and observed that, increase of defect degree shifts stability region to lower excitation frequencies.

The dynamic buckling of viscoelastic sandwich truncated nanocomposite conical shells under moisture, temperature, and magnetic field effects, crucial for aerospace applications addressed in Ref. [53]. They observed that the increase of moisture and temperature lead to dynamic instability at lower excitation frequencies.

BehroozKeshtegar et al. [54] investigated dynamic buckling in viscoelastic carbon nanocones (CNCs) under magnetic and thermal loads, relevant for nano-electro-mechanical systems (NEMS) like scanning probe microscopy. Bolotin's method and differential quadrature method (DQM) are used to analyze dynamic instability regions (DIRs), and revealed the study that increasing strain gradient parameter shifts DIR to higher frequencies, with magnetic loads positively impacting CNCs' DIR.

To summarize, the analysis of bi-directional FGPs is a complex undertaking, necessitating accurate predictions of their buckling behavior and consideration of the effects of porosity. This paper explores the buckling behavior of inplane bi-directional FGPs with uniform porosity using higher order theory with only five unknowns.

In this investigation, the inplane 2-D FG plate material properties are gradually varying in two directions (η_1 and η_2), while maintaining a constant Poissons ratio. The Lagrange's equations are used to derive the equations of motion, and both inplane and transverse displacements are articulated as algebraic polynomial series, incorporating admissible functions to satisfy boundary conditions. These admissible functions are derived using Pascal's triangle. The accurateness of this theory is judged against numerical results found in existing literature. The study delves into the impact of thickness ratio's, aspect ratio's, gradation indexes, and porosity on the buckling behavior of in-plane bi-directional FGPs under both uniaxial and biaxial compression.

2. Problem Formulation

Fig 1 shows an IBFGP Pate with physical dimensions' length, *a;* width, *b;* and thickness, *h.* The plate modulus of elasticity is assumed to alter both in η_1 and η_2-directions by means of the rule of the mixture as.

$$E(\eta_1,\eta_2) = (E_c - E_m)\left(\frac{\eta_1}{a}\right)^{\zeta_1}\left(\frac{\eta_2}{b}\right)^{\zeta_2} + E_m - \frac{\Phi}{2}(E_c + E_m) \quad (1)$$

The porosities can be distributed evenly in the plate.

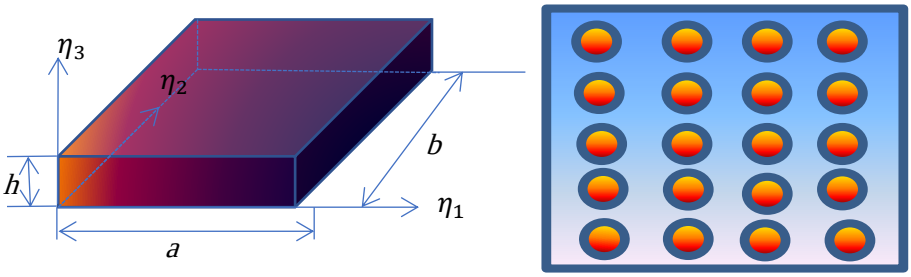

Fig 1: Representation of an in-plane bi-directional FGP with even porosity distribution

Where, E_c and E_m, are Young's Modulus of the Ceramic and metallic materials, respectively, while $\zeta_1$and ζ_2 are the *g*radation indexes along the η_1-direction and η_2 direction respectively, and Φ is the porosity volume fraction. $\Phi = 0$ represents the perfect in-plane bi-directional Functionally Graded plate. The effective Young's modulus (E_{eff}) of in-plane bi-directional FGP varied with the constituent component material properties presented in Table 1. The E_{eff} is

calculated by the Eqs. (1) and is shown in Figs 2-3 for the specific case of $\zeta_1 = 5, \zeta_2 = 2$ thickness ratio, a/h=10 and $\Phi = 0, 0.1$ and 0.2.

$$E_{eff} = \frac{\int_V E(\eta_1,\eta_2)dV}{V} \tag{2}$$

Table 1: Properties of material [55].

Properties of the material	Al_2O_3 (Ceramic)	SiC (Ceramic)	Al (Metal)
E (GPa)	380	420	70
μ	0.3	0.3	0.3

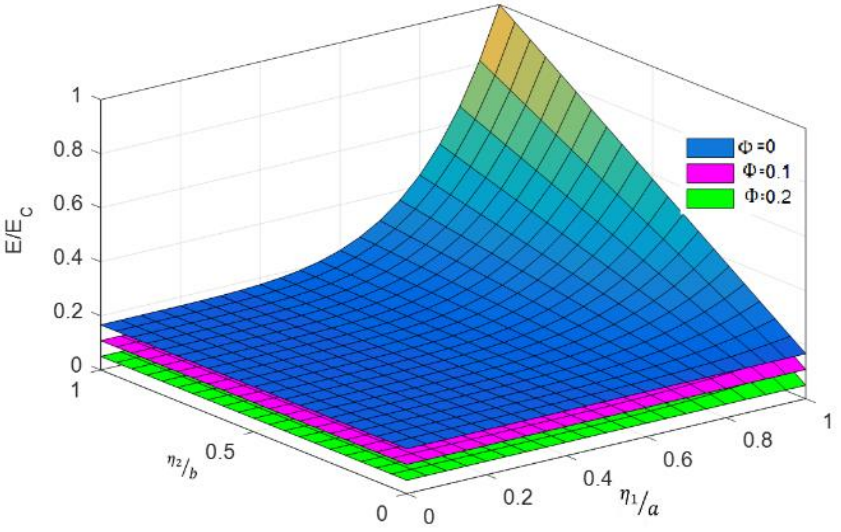

Fig 2: Young's Modulus of in-plane bi-directional FGP with even porosity for different volume fraction of porosity

In addition, Fig 3 shows the alteration of effective Young's modulus, $E\ (\eta_1, \eta_2)$ of in-plane bi-directional FG porous plate (from Eq. (2)). From Fig 3, it is evident that the Young's modulus decreases as the volume fraction of porosity increases and gradation index*es* ζ_1 and ζ_2 .

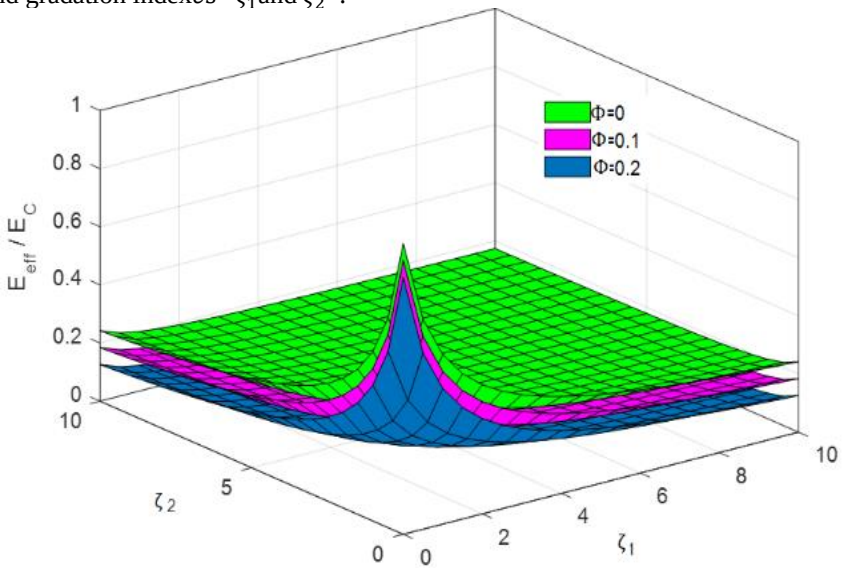

Fig 3: Young's modulus of the in-plane bi-directional FGP with even porosity as a function of ζ_1, ζ_2 and Φ

2.1. Kinematics

This paper uses the generalized shear deformation theory proposed by Zenkour [56]. The displacement field of this theory can be written as:

$$\bar{u}\,(\eta_1,\eta_2) = u\; -\; \eta_3 \frac{\partial w}{\partial \eta_1}\; +\; \emptyset(\eta_3)\,\emptyset_{\eta_1} \tag{3a}$$

$$\bar{v}\,(\eta_1,\eta_2) = u\; -\; \eta_3\; \frac{\partial w}{\partial \eta_2}\; +\; \emptyset(\eta_3)\,\emptyset_{\eta_2} \tag{3b}$$

$$\overline{w} = w \tag{3c}$$

$$\text{Where } \emptyset(\eta_3) = \frac{5}{4}\eta_3\left(1 - \frac{4}{3}\left[\frac{\eta_3}{h}\right]^2\right) \tag{3d}$$

The kinematic realtions can be derived as follows:

$$\epsilon_{\eta_1} = \frac{\partial \bar{u}(\eta_1,\eta_2)}{\partial \eta_1} = \frac{\partial u}{\partial \eta_1} - \eta_3 \frac{\partial^2 w}{\partial {\eta_1}^2} + \emptyset(\eta_3)\frac{\partial \emptyset_{\eta_1}}{\partial \eta_1} \tag{4a}$$

$$\epsilon_{\eta_2} = \frac{\partial \bar{v}(\eta_1,\eta_2)}{\partial\, \eta_2} = \frac{\partial v}{\partial\, \eta_2} - \eta_3\; \frac{\partial^2 w}{\partial\, {\eta_2}^2} + \emptyset(\eta_3)\; \frac{\partial \emptyset_{\eta_2}}{\partial\, \eta_2} \tag{4b}$$

$$\epsilon_{\eta_1\eta_2} = \frac{\partial \bar{u}(\eta_1,\eta_2)}{\partial \eta_2} + \frac{\partial \bar{v}(\eta_1,\eta_2)}{\partial \eta_1}$$

$$= \frac{\partial u}{\partial \eta_2} + \frac{\partial v}{\partial \eta_1} - 2\eta_3 \frac{\partial^2 w}{\partial \eta_1 \partial \eta_2} + \emptyset(\,\eta_3)\left(\frac{\partial \emptyset_{\eta_1}}{\partial \eta_2} + \frac{\partial \emptyset_{\eta_2}}{\partial \eta_1}\right) \tag{4c}$$

$$\epsilon_{\eta_1\eta_3} = \frac{\partial \emptyset(\eta_3)}{\partial \eta_3}\; \emptyset_{\eta_1} \tag{4d}$$

$$\epsilon_{\eta_2\eta_3} = \frac{\partial \emptyset(\eta_3)}{\partial \eta_3}\; \emptyset_{\eta_2} \tag{4e}$$

Transverse shear strains are integrated into Equation (3d), which accounts for the transverse shear strain distribution across the plate's thickness. Consequently, the current theory eliminates the necessity for a shear correction factor.

We will compute the gradients of $\bar{u}$, and $\bar{v}$ with respect to $\eta_1\ and\ \eta_2$ respectively the gradients will give us the components of the infinitesimal rotation vector$\vec{\omega}$

$$\vec{\omega} = \begin{bmatrix} \omega_x \\ \omega_y \\ \omega_z \end{bmatrix}$$

Now, let us derive the expressions for $\omega_x, \omega_y, and\ \ \omega_z$ using the displacement equations

ω_x:

From the displacement equations

$$\omega_x = -\frac{\partial \bar{u}}{\partial \eta_2} = -\frac{\partial}{\partial \eta_2}\left(u\; -\; \eta_3 \frac{\partial w}{\partial \eta_1}\; +\; \emptyset(\eta_3)\,\emptyset_{\eta_1}\right)$$

Simplifying the terms, we get

$$\omega_x = \eta_3 \frac{\partial^2 w}{\partial \eta_1 \eta_2} - \frac{\partial}{\partial \eta_2}\left(\,\emptyset(\eta_3)\,\emptyset_{\eta_1}\right)$$

ω_y:

$$\omega_y = -\frac{\partial \bar{u}}{\partial \eta_1} = -\frac{\partial}{\partial \eta_1}\left(u\; -\; \eta_3 \frac{\partial w}{\partial \eta_2}\; +\; \emptyset(\eta_3)\,\emptyset_{\eta_2}\right)$$

Simplifying the terms, we get

$$\omega_y = -\eta_3 \frac{\partial^2 w}{\partial \eta_1 \eta_2} - \frac{\partial}{\partial \eta_1}\left(\,\emptyset(\eta_3)\,\emptyset_{\eta_2}\right)$$

ω_z:

$$\omega_z = -\frac{\partial \overline{w}}{\partial \eta_1} = 0 \quad (as\ \overline{w} = w)$$

2.2. Linear Constitutive Relations

The stress and strain relationships for in-plane bidirectional FGPs are expressed as follows:

$$\sigma_{\eta_1} = Q_{11}\epsilon_{\eta_1} + Q_{12}\epsilon_{\eta_2} \tag{5a}$$

$$\sigma_{\eta_2} = Q_{12}\epsilon_{\eta_1} + Q_{11}\epsilon_{\eta_2} \tag{5b}$$

$$[\sigma_{\eta_1\eta_2}\ \sigma_{\eta_1\eta_3}\ \sigma_{\eta_2\eta_3}] = Q_{44}[\epsilon_{\eta_1\eta_2}\ \epsilon_{\eta_1\eta_3}\ \epsilon_{\eta_2\eta_3}] \tag{5c}$$

$$Q_{11} = \frac{E(\eta_1,\eta_2)}{1-\mu^2}, Q_{12} = \mu Q_{11}, Q_{44} = \frac{E(\eta_1,\eta_2)}{2(1+\mu)}$$

In which, $\{\sigma_{\eta_1}, \sigma_{\eta_2}, \sigma_{\eta_1\eta_2}, \sigma_{\eta_1\eta_3}, \sigma_{\eta_2\eta_3}\}$ are the stresses and $\{\epsilon_{\eta_1}, \epsilon_{\eta_2}, \epsilon_{\eta_1\eta_2}, \epsilon_{\eta_1\eta_3}, \epsilon_{\eta_2\eta_3}\}$ are the strains in regards to the plate's coordinate system.

2.3. Formulation of Buckling problem

The expression for the strain energy of the in-plane bidirectional functionally graded plate is as follows:

$$U = \frac{1}{2}\int_V [\sigma_{\eta_1}\epsilon_{\eta_1} + \sigma_{\eta_2}\epsilon_{\eta_2} + \sigma_{\eta_1\eta_2}\epsilon_{\eta_1\eta_2} + \sigma_{\eta_1\eta_3}\epsilon_{\eta_1\eta_3} + \sigma_{\eta_2\eta_3}\epsilon_{\eta_2\eta_3}]\, dV \quad (6)$$

By substituting equations (4-5) into equation (6), the strain energy equation can be expressed as:

$$U = \frac{1}{2}\int_V \Bigg[Q_{11}\Bigg(\left[\frac{\partial u}{\partial \eta_1}\right]^2 + \left[\frac{\partial v}{\partial \eta_2}\right]^2 - 2\eta_3\left[\frac{\partial u}{\partial \eta_1}\frac{\partial^2 w}{\partial {\eta_1}^2} + \frac{\partial v}{\partial \eta_2}\frac{\partial^2 w}{\partial {\eta_2}^2}\right] + 2\,\emptyset(\eta_3)\left[\frac{\partial u}{\partial \eta_1}\frac{\partial \emptyset_{\eta_1}}{\partial \eta_1} + \frac{\partial v}{\partial \eta_2}\frac{\partial \emptyset_{\eta_2}}{\partial \eta_2}\right] + {\eta_3}^2\Bigg(\left[\frac{\partial^2 w}{\partial {\eta_1}^2}\right]^2 + \left[\frac{\partial^2 w}{\partial {\eta_2}^2}\right]^2\Bigg) - 2\eta_3\emptyset(\eta_3)\left[\frac{\partial \emptyset_{\eta_1}}{\partial \eta_1}\frac{\partial^2 w}{\partial {\eta_1}^2} + \frac{\partial \emptyset_{\eta_2}}{\partial \eta_2}\frac{\partial^2 w}{\partial {\eta_2}^2}\right] + \left(\emptyset(\eta_3)\right)^2\left(\left[\frac{\partial \emptyset_{\eta_1}}{\partial \eta_1}\right]^2 + \left[\frac{\partial \emptyset_{\eta_2}}{\partial \eta_2}\right]^2\right)\Bigg) + 2Q_{12}\Bigg(\frac{\partial u}{\partial \eta_1}\frac{\partial v}{\partial \eta_2} - \eta_3\left[\frac{\partial v}{\partial \eta_2}\frac{\partial^2 w}{\partial {\eta_1}^2} + \frac{\partial u}{\partial \eta_1}\frac{\partial^2 w}{\partial {\eta_2}^2}\right] + \emptyset(\eta_3)\left[\frac{\partial \emptyset_{\eta_1}}{\partial \eta_1}\frac{\partial v}{\partial \eta_2} + \frac{\partial u}{\partial \eta_1}\frac{\partial \emptyset_{\eta_2}}{\partial \eta_2}\right] + {\eta_3}^2\left[\frac{\partial^2 w}{\partial {\eta_1}^2}\frac{\partial^2 w}{\partial {\eta_2}^2}\right] - \eta_3\emptyset(\eta_3)\left[\frac{\partial \emptyset_{\eta_1}}{\partial \eta_1}\frac{\partial^2 w}{\partial {\eta_2}^2} + \frac{\partial \emptyset_{\eta_2}}{\partial \eta_2}\frac{\partial^2 w}{\partial {\eta_1}^2}\right] + \left(\emptyset(z\eta_3)\right)^2\frac{\partial \emptyset_{\eta_1}}{\partial \eta_1}\frac{\partial \emptyset_{\eta_2}}{\partial \eta_2}\Bigg) + Q_{44}\Bigg(\left[\frac{\partial u}{\partial \eta_2} + \frac{\partial v}{\partial \eta_1}\right]^2 - 4\eta_3\frac{\partial^2 w}{\partial \eta_1 \partial \eta_2}\left[\frac{\partial u}{\partial \eta_2} + \frac{\partial v}{\partial \eta_1}\right] + 2\emptyset(\eta_3)\left(\left[\frac{\partial \emptyset_{\eta_1}}{\partial \eta_2} + \frac{\partial \emptyset_{\eta_2}}{\partial \eta_1}\right]\left[\frac{\partial u}{\partial \eta_2} + \frac{\partial v}{\partial \eta_1}\right]\right) - 4z\emptyset(\eta_3)\frac{\partial^2 w}{\partial \eta_1 \partial \eta_2}\left[\frac{\partial \emptyset_{\eta_1}}{\partial \eta_2} + \frac{\partial \emptyset_{\eta_2}}{\partial \eta_1}\right] + 4{\eta_3}^2\left[\frac{\partial^2 w}{\partial \eta_1 \partial \eta_2}\right]^2 + \left(\emptyset(\eta_3)\right)^2\left(\left[\frac{\partial \emptyset_{\eta_1}}{\partial \eta_2}\right]^2 + \left[\frac{\partial \emptyset_y}{\partial \eta_1}\right]^2\right)^2 + \left(\frac{\partial \emptyset(\eta_3)}{\partial \eta_3}\right)^2\left[{\emptyset_{\eta_1}}^2 + {\emptyset_{\eta_2}}^2\right]\Bigg)\Bigg] dV \quad (7)$$

The work done by in-plane pre-buckling forces can be stated as:

$$\mathrm{V} = \int_A \left(N^0_{\eta_1}\left(\frac{\partial w}{\partial \eta_1}\right)^2 + N^0_{\eta_2}\left(\frac{\partial w}{\partial \eta_2}\right)^2\right) d\eta_1 d\eta_2 \quad (8)$$

Where ($N^0_{\eta_1}, N^0_{\eta_2}$ are inplane prebuckling forces.

Governing equations are derived through the application of the minimum potential energy principle, which can be stated analytically as follows.

$$\delta(U + V) = 0 \quad (9)$$

Inplane and transverse displacement functions namely $u\,(\eta_1,\eta_2)$, $v\,(\eta_1,\eta_2)$, $w\,(\eta_1,\eta_2)$, $\emptyset_{\eta_1}(\eta_1,\eta_2)$ and $\emptyset_{\eta_2}(\eta_1,\eta_2)$ are represented using polynomial series that conform to boundary conditions is given as:

$$u(\eta_1,\eta_2) = \sum_{i=1}^{n} C_i\, \phi_i(\eta_1,\eta_2);$$

$$\phi_i(\eta_1,\eta_2) = {\eta_1}^{p_u}{\eta_2}^{q_u}(\eta_1 - a)^{r_u}(\eta_2 - b)^{s_u}\, \psi_i^u(\eta_1,\eta_2) \quad (10a)$$

$$v(\eta_1,\eta_2) = \sum_{i=1}^{n} C_j\, \lambda_i(\eta_1,\eta_2);$$

$$\lambda_i(\eta_1,\eta_2) = {\eta_1}^{p_v}{\eta_2}^{q_v}(\eta_1 - a)^{r_v}(\eta_2 - b)^{s_v}\, \psi_j^v(\eta_1,\eta_2) \quad (10b)$$

$$w(\eta_1,\eta_2) = \sum_{i=1}^{n} C_k\Delta_i(\eta_1,\eta_2);$$

$$\Delta_i(\eta_1,\eta_2) = {\eta_1}^{p_w}{\eta_2}^{q_w}(\eta_1 - a)^{r_w}(\eta_2 - b)^{s_w}\, \psi_k^w(\eta_1,\eta_2) \quad (10c)$$

$$\emptyset_{\eta_1}(\eta_1,\eta_2) = \sum_{i=1}^{n}\frac{1}{a} C_l\, \Omega_i(\eta_1,\eta_2);$$

$$\Omega_i(\eta_1,\eta_2) = {\eta_1}^{p_{\emptyset\eta_1}}{\eta_2}^{q_{\emptyset\eta_1}}(\eta_1 - a)^{r_{\emptyset\eta_1}}(\eta_2 - b)^{s_{\emptyset\eta_1}}\, \psi_l^{\emptyset\eta_1}(\eta_1,\eta_2) \quad (10d)$$

$$\emptyset_{\eta_2}(\eta_1,\eta_2) = \sum_{i=1}^{n}\frac{1}{b} C_m\, \xi_i(\eta_1,\eta_2);$$

$$\xi_i(\eta_1,\eta_2) = {\eta_1}^{p_{\emptyset\eta_2}}{\eta_2}^{q_{\emptyset\eta_2}}(\eta_1 - a)^{r_{\emptyset\eta_2}}(\eta_2 - b)^{s_{\emptyset\eta_2}}\, \psi_m^{\emptyset\eta_2}(\eta_1,\eta_2) \quad (10e)$$

$\phi_i(\eta_1,\eta_2), \lambda_i(\eta_1,\eta_2), \Delta_i(\eta_1,\eta_2), \Omega_i(x,y)\ and\ \xi_i(\eta_1,\eta_2)$ are the shape functions, $p_\Upsilon, q_\Upsilon, r_\Upsilon, s_\Upsilon$ ($\Upsilon = \mathrm{u, v, w}, \emptyset_{\eta_1}, \emptyset_{\eta_2}$) are govern the imposition of different boundary conditions. For simple support, these exponents assume values of either 0 or 1 at the sides η_1=0, a and η_2=0, b. The specific boundary exponents are as follows:

p_u=0;r_u=0;p_v=1;r_v=1;p_w=1;r_w=1;pϕ_{η_1}=0;rϕ_{η_1}=0;pϕ_{η_2}=1;rϕ_{η_2}=1;

q_u=1;s_u=1;q_v=0;s_v=0;q_w=1;s_w=1;qϕ_{η_1}=1;sϕ_{η_1}=1;qϕ_{η_2}=0;sϕ_{η_2}=0;

The 21 admissible functions of ψ_i (i=1, 2, 3……21) are derived using Pascal's triangle and expressed as :

$$\psi_1 = 1;\ \psi_2 = \eta_1;\psi_3 = \eta_2;\psi_4 = {\eta_1}^2;\psi_5 = \eta_1\eta_2;\psi_6 = {\eta_2}^2;\psi_7 = {\eta_1}^3;\ \psi_8 = {\eta_1}^2\eta_2;\psi_9 = \eta_1{\eta_2}^2;\psi_{10} = {\eta_2}^3;\psi_{11} = {\eta_1}^4;\psi_{12} = {\eta_1}^3\eta_2;$$

$$\psi_{13} = {\eta_1}^2\eta_2;\psi_{14} = \eta_1{\eta_2}^3;\psi_{15} = {\eta_2}^4;\psi_{16} = {\eta_1}^5;\quad \psi_{17} = {\eta_1}^4\eta_2\ ;\ \psi_{18} = {\eta_1}^3{\eta_2}^2\ ;\ \psi_{19} = {\eta_1}^2{\eta_2}^3\ ;\ \psi_{20} = {\eta_1}^1{\eta_2}^4;\psi_{21} = {\eta_2}^5; \quad (11)$$

The closed form solution can be obtained by the substitution of Eqs. (7), (8) and (10) into Eqs. (9) as

$$[\boldsymbol{S}] - \chi[\boldsymbol{M}]\begin{Bmatrix}\{u\}\\ \{v\}\\ \{w\}\\ \{\emptyset_{\eta_1}\}\\ \{\emptyset_{\eta_2}\}\end{Bmatrix} = \{\mathbf{0}\} \quad (12)$$

Where **[S]** is the stiffness matrices and **[M]** are the in-plane force matrix. The elements of **[S]** and **[M] are** given as

$$S_{11}(i,j)=\int_0^a\int_0^b\int_{-h/2}^{h/2}\left(Q_{11}\emptyset_{i,\eta_1}\emptyset_{j,\eta_1}+Q_{44}\emptyset_{i,\eta_2}\emptyset_{j,\eta_2}\right)d\eta_3 d\eta_2 d\eta_1$$

$$S_{12}(i,j)=\int_0^a\int_0^b\int_{-h/2}^{h/2}\left(Q_{12}\emptyset_{i,\eta_1}\lambda_{j,\eta_2}+Q_{44}\emptyset_{i,\eta_2}\lambda_{j,\eta_1}\right)d\eta_3 d\eta_2 d\eta_1$$

$$S_{13}(i,j)=-\int_0^a\int_0^b\int_{-h/2}^{h/2}\eta_3\left(Q_{11}\emptyset_{i,\eta_1}\Delta_{j,\eta_1\eta_1}+Q_{12}\emptyset_{i,\eta_1}\Delta_{j,\eta_2\eta_2}+2Q_{44}\emptyset_{i,\eta_2}\Delta_{j,\eta_1\eta_2}\right)d\eta_3 d\eta_2 d\eta_1$$

$$S_{14}(i,j)=\frac{1}{a}\int_0^a\int_0^b\int_{-h/2}^{h/2}\emptyset(\eta_3)\left(Q_{11}\emptyset_{i,\eta_1}\Omega_{j,\eta_1}+Q_{44}\emptyset_{i,\eta_2}\Omega_{j,\eta_2}\right)d\eta_3 d\eta_2 d\eta_1$$

$$S_{15}(i,j)=\frac{1}{b}\int_0^a\int_0^b\int_{-h/2}^{h/2}\emptyset(\eta_3)\left(Q_{12}\emptyset_{i,\eta_1}\xi_{j,\eta_2}+Q_{44}\emptyset_{i,\eta_2}\xi_{j,\eta_1}\right)d\eta_3 d\eta_2 d\eta_1$$

$$S_{22}(i,j)=\int_0^a\int_0^b\int_{-h/2}^{h/2}\left(Q_{11}\lambda_{i,\eta_2}\lambda_{j,\eta_2}+Q_{44}\lambda_{i,\eta_1}\lambda_{j,\eta_1}\right)d\eta_3 d\eta_2 d\eta_1$$

$$S_{23}(i,j)=-\int_0^a\int_0^b\int_{-h/2}^{h/2}\eta_3\left(Q_{12}\lambda_{i,\eta_2}\Delta_{j,\eta_1\eta_1}+Q_{11}\lambda_{i,\eta_2}\Delta_{j,\eta_2\eta_2}+2Q_{44}\lambda_{i,\eta_1}\Delta_{j,\eta_1\eta_2}\right)d\eta_3 d\eta_2 d\eta_1$$

$$S_{24}(i,j)=\frac{1}{a}\int_0^a\int_0^b\int_{-h/2}^{h/2}\emptyset(\eta_3)\left(Q_{12}\lambda_{i,\eta_2}\Omega_{j,\eta_1}+Q_{44}\lambda_{i,\eta_1}\Omega_{j,\eta_2}\right)d\eta_3 d\eta_2 d\eta_1$$

$$S_{25}(i,j)=\frac{1}{b}\int_0^a\int_0^b\int_{-h/2}^{h/2}\emptyset(\eta_3)\left(Q_{11}\lambda_{i,\eta_2}\xi_{j,\eta_2}+Q_{44}\lambda_{i,\eta_1}\xi_{j,\eta_1}\right)d\eta_3 d\eta_2 d\eta_1$$

$$S_{33}(i,j)=\int_0^a\int_0^b\int_{-h/2}^{h/2}{\eta_3}^2\left(Q_{11}\left(\Delta_{i,\eta_1\eta_1}\Delta_{j,\eta_1\eta_1}+\Delta_{i,\eta_2\eta_2}\Delta_{j,\eta_2\eta_2}\right)+2Q_{12}\Delta_{i,\eta_1\eta_1}\Delta_{j,\eta_2\eta_2}+4Q_{44}\Delta_{i,\eta_1\eta_2}\Delta_{j,\eta_1\eta_2}\right)d\eta_3 d\eta_2 d\eta_1$$

$$S_{34}(i,j)=-\frac{1}{a}\int_0^a\int_0^b\int_{-h/2}^{h/2}\eta_3\emptyset(\eta_3)\left(Q_{11}\Delta_{i,\eta_1\eta_1}\Omega_{j,\eta_1}+Q_{12}\Delta_{i,\eta_2\eta_2}\Omega_{j,\eta_1}+2Q_{44}\Delta_{i,\eta_1\eta_2}\Omega_{j,\eta_2}\right)d\eta_3 d\eta_2 d\eta_1$$

$$S_{35}(i,j)=-\frac{1}{b}\int_0^a\int_0^b\int_{-h/2}^{h/2}\eta_3\emptyset(\eta_3)\left(Q_{12}\Delta_{i,\eta_1\eta_1}\xi_{j,\eta_2}+Q_{11}\Delta_{i,\eta_2\eta_2}\xi_{j,\eta_2}+2Q_{44}\Delta_{i,\eta_1\eta_2}\xi_{j,\eta_1}\right)d\eta_3 d\eta_2 d\eta_1$$

$$S_{44}(i,j)=\frac{1}{a^2}\int_0^a\int_0^b\int_{-h/2}^{h/2}\left(\emptyset(\eta_3)\right)^2\left(Q_{11}\Omega_{i,\eta_1}\Omega_{j,\eta_1}+Q_{44}\Omega_{i,\eta_2}\Omega_{j,\eta_2}\right)+Q_{44}\left[\frac{\partial\emptyset(\eta_3)}{\partial\eta_3}\right]^2\Omega_i\Omega_j d\eta_3 d\eta_2 d\eta_1$$

$$S_{45}(i,j)=\frac{1}{ab}\int_0^a\int_0^b\int_{-h/2}^{h/2}\left(\emptyset(\eta_3)\right)^2\left(Q_{12}\Omega_{i,\eta_1}\xi_{j,\eta_2}+Q_{44}\Omega_{i,\eta_2}\Omega_{j,\eta_2}\right)+Q_{44}\Omega_{i,\eta_2}\xi_{j,\eta_1}d\eta_3 d\eta_2 d\eta_1$$

$$S_{55}(i,j)=\frac{1}{b^2}\int_0^a\int_0^b\int_{-h/2}^{h/2}\left(\emptyset(\eta_3)\right)^2\left(Q_{11}\xi_{i,\eta_2}\xi_{j,\eta_2}+Q_{44}\xi_{i,\eta_1}\xi_{j,\eta_1}\right)+Q_{44}\left[\frac{\partial\emptyset(\eta_3)}{\partial\eta_3}\right]^2\xi_i\xi_j d\eta_3 d\eta_2 d\eta_1$$

$$M_{11}(i,j) = M_{12}(i,j) = M_{13}(i,j) = M_{14}(i,j) = M_{15}(i,j) = M_{22}(i,j) = M_{23}(i,j) = M_{24}(i,j) = M_{25}(i,j) = M_{34}(i,j) = M_{35}(i,j) = M_{44}(i,j) = M_{45}(i,j) = M_{55}(i,j)0$$

$M_{33}(i,j) = \int_0^a \int_0^b \varsigma_1 \Delta_{i,\eta_1} \Delta_{j,\eta_1} + \varsigma_2 \Delta_{i,\eta_2} \Delta_{j,\eta_2}) d\eta_1 d\eta_2$, i,j=1, 2..

$\varsigma_1 = 1$ and $\varsigma_2 = 0$ for uni $-$ axial compression; $\varsigma_1 = 1$ and $\varsigma_2 = 1$ for bi $-$ axial compression are considered for the analysis. To obtain the critical buckling loads Eq. (12) is solved by taking $|[\boldsymbol{S}] - \chi[\boldsymbol{M}]| = 0$

3. Results and Discussion

This section addresses the impact of a/h, b/a,, ζ_1, ζ_2 and , Φ, and in-plane loads on the buckling analyses of bidirectional FGPs.

The numerical study is carried for simple support beam conditions and are set as. v=0, w = 0, $\emptyset_{\eta_2} = 0$ @ $\eta_1 = 0$, a; u =0, w = 0, $\emptyset_{\eta_1} = 0$ @ $\eta_2 = 0$, b considering plate material properties given in Table 1. The critical buckling load results are portrayed in dimensionless form as:

Dimensionless buckling load, $\bar{N} = N_{cr} \frac{a^2}{E_m h^3}$

To validate the present higher order theory, comparison studies are performed. Results are potrayed in dimensionless form in Table 2 and assessed with Sidda Reddy et al. [16], Thai and Chai. [55], Thai and Kim [57].

From an accurateness point, 21 admissible functions of ψ_i are considered in examining the buckling behaviour of simply supported bidirectional FG porous plates. From Table 2, it is seen that the present theory results with 21 number of admissible functions are well agreeing with the results of Thai and Chai. [55], Thai and Kim [57]. Therefore, the findings from the present theory should serve as the reference results for future comparative analyses.

Table 2: Dimensionless critical buckling load ($\bar{N}$) of simply supported Al/Al_2O_3 plate subjected to both uni-axial and bi-axial compression for a/h =10, b/a =1

Uniaxial Compression						
		Volume fraction Exponents				
No. of admissible functions	**Theory**	**0**	**1**	**2**	**5**	**10**
21	**Present**	**18.5785**	**9.3391**	**7.2631**	**6.0353**	**5.4529**
	Ref. [16]	18.54	9.299	7.21	5.99	5.42
	Ref. [55]	18.5785	9.3391	7.2631	6.0353	5.4528
	Ref. [57]	18.5785	9.3391	7.2631	6.0353	5.4528
	Ref. [58], n = 3	18.5785	9.3391	7.2631	6.0353	5.4528
	Ref. [58], n = 5	18.5983	9.3476	7.2744	6.0593	5.47
	Ref. [58], n = 7	18.6224	9.3578	7.2855	6.078	5.4869
	Ref. [58], n = 9	18.6409	9.3657	7.2938	6.0911	5.4999
No. of admissible functions		**Biaxial compression**				
21	**Present**	**9.2893**	**4.6696**	**3.6315**	**3.0177**	**2.7264**
	Ref. [16]	9.273	4.650	3.608	2.998	2.715
	Ref. [55]	9.2893	4.6696	3.6315	3.0177	2.7264
	Ref. [57]	9.2893	4.6695	3.6315	3.0177	2.7264
	Ref. [58], n = 3	9.2893	4.6695	3.6315	3.0177	2.7264
	Ref. [58], n = 5	9.2992	4.6738	3.6372	3.0297	2.735
	Ref. [58], n = 7	9.3112	4.6789	3.6427	3.039	2.7435
	Ref. [58], n = 9	9.3205	4.6829	3.6469	3.0455	2.7499

3.1. In-plane bi-directional critical buckling loads under uni-axial compression

In Table 3, the dimensionless critical buckling loads are presented for rectangular plates, b/a =2 with, a/h =10, gradation indexes ζ_1 and ζ_2= {0,1,2,5}, the volume fraction of porosity Φ= {0,0.1,0.2}, under uniaxial compression.

From Table 3, it is observed that, the dimensionless critical buckling loads of in-plane bidirectional functionally graded plates are decreasing with the increase of gradation indexes and porosity volume fraction. The reason can be

attributed to the variation in material properties like effective Young's modulus drastically in the η_1 and η_2 directions as shown in Fig 3. As the gradation index and porosity volume fraction increase, the material within the plate becomes more heterogeneous and porous. This leads to reduction of structural integrity and plate's stiffness and resistance to buckling, making it more susceptible to critical loads.

The effect of a/h, ζ_1 , ζ_2, and Φ on the dimensionless critical buckling loads under uniaxial compression are presented in Table 4 and Fig 4.

From the Table 4 and Fig 4, it is seen that, the increase of a /h, increases the critical buckling loads and decreases with the increase of ζ_1 , ζ_2, and Φ. This is because, a larger a/h results in a slenderer and less stocky structure. This increased slenderness allows the structure to better distribute and resist applied loads, reducing the risk of buckling. On the other hand, as the gradation index and porosity volume fraction increase, the material within the structure becomes more heterogeneous and porous, which weakens its overall structural integrity. So, the combined effect is that while an increased side-to-thickness ratio enhances stability, higher gradation indexes and porosity diminish it due to weakened material properties.

Table 5 and Fig 5 shows the changes in the dimensionless critical buckling load when subjected to uniaxial compression for various b/a ratio, ζ_1 , ζ_2, and Φ. From the Table 5 & Fig 5, it is noticed that, the increase of aspect ratio decreases the critical buckling loads and decreases with the increase of gradation indexes and porosity volume fraction. The reason is, the increase of b/a ratio, ζ_1 , ζ_2, and Φ, decreases the overall plate's stiffness, create material heterogeneity and hence more prone to buckling. This increased heterogeneity results in non-uniform stress distribution, particularly in the longitudinal direction, which magnifies the buckling susceptibility. Furthermore, the presence of porosity decreases the plate's load carrying capacity, as porous regions act as stress concentration points and introduce local instabilities. Collectively, these effects lead to a significant reduction in the critical buckling loads as b/a ratio, ζ_1 , ζ_2, and Φ increase, making the plate more vulnerable to buckling under critical loads. The critical buckling load is same at two points b/a ≅0.75 for Φ =0.2; ζ_1=1; ζ_2 =1 & Φ =0.1; ζ_1=2; ζ_2 =5 and b/a ≅0.53 for Φ =0; ζ_1=2; ζ_2 =5 & Φ =0.1; ζ_1=1; ζ_2 =1.

Table 3: Dimensionless critical buckling loads of rectangular plates, a/h=10 and b/a=2 under uniaxial compression

ζ_2	Φ	ζ_1			
		0	1	2	5
0	0	8.18484	4.15133	2.77344	1.87645
	0.1	7.70739	3.56367	2.1649	1.33927
	0.2	7.22994	2.89736	1.45822	0.76009
1	0	4.1801	2.68134	2.10432	1.64783
	0.1	3.61013	2.12537	1.56081	1.14091
	0.2	2.99136	1.50908	0.96317	0.60985
2	0	2.77988	2.10714	1.82144	1.55995
	0.1	2.18362	1.56595	1.3004	1.06378
	0.2	1.50975	0.97376	0.74385	0.55094
5	0	1.82525	1.6329	1.55144	1.46361
	0.1	1.28533	1.12496	1.05448	0.97735
	0.2	0.70603	0.59279	0.54061	0.48266

3.2. In-plane bi-directional critical buckling loads under bi-axial compression

The effect of a/h, ζ_1 , ζ_2, and Φ on the dimensionless critical buckling load under bi-axial compression are presented in Tables 6-8 and shown in Figs 6-8.

From the Table 6 and Fig 6, it is seen that, the increase of side to thickness ratio, increases the critical buckling loads and decreases with the increase of gradation indexes and volume fraction of porosity. The similar behaviour is observed in uniaxial compression also. Moreover, the dimensionless critical buckling load of plate subjected to uniaxial compression is greater compared to biaxial compression. The reason is, uniaxial compression allows the plate to deform in only one direction, which is more resistant to buckling compared to biaxial compression, where the plate is subjected to deformation in two orthogonal directions. In uniaxial compression, the plate can distribute the compressive load more efficiently, with less risk of lateral instability, while in biaxial compression, the load is applied in two directions, leading to a higher likelihood of buckling due to the increased stress and deformations in both directions. Therefore, the critical buckling load is higher in uniaxial compression because it offers a more stable load-

bearing configuration.

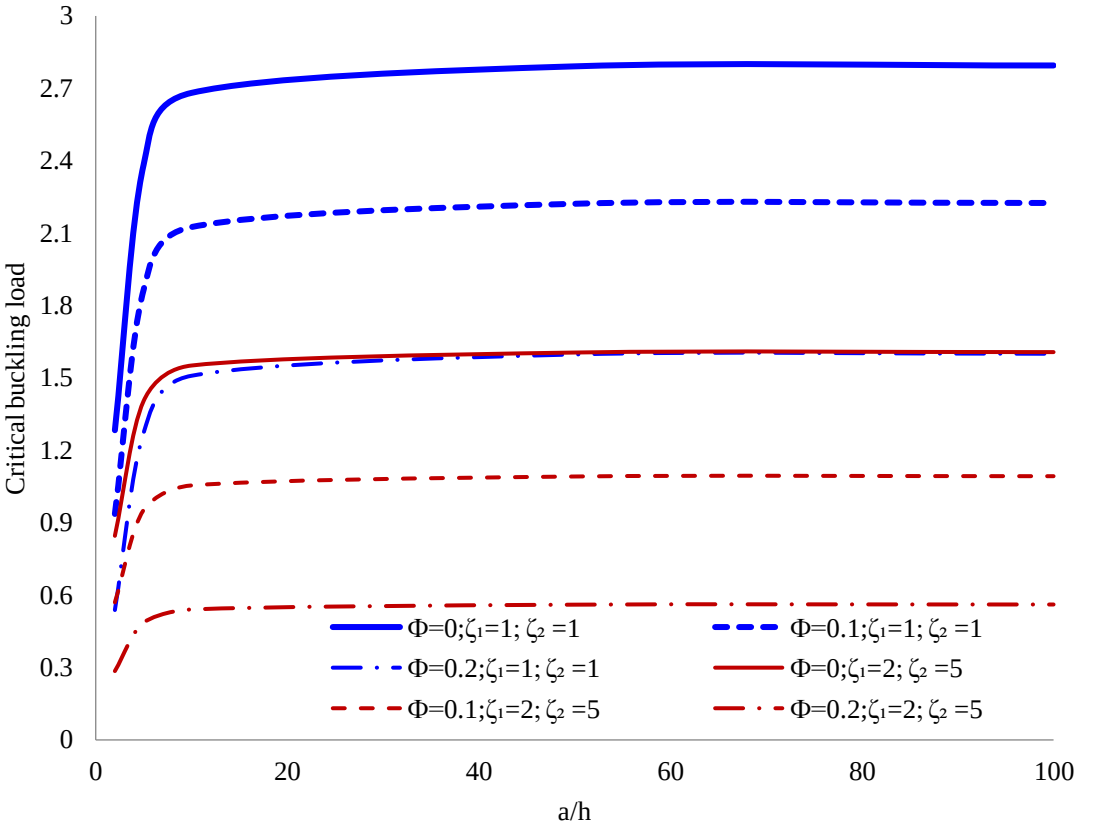

Fig 4: Influence of side to thickness ratio (a/h), gradation indexes and volume fraction of porosity on inplane bidirectional plate, b/a=2

Table 4: Influence of side-to- thickness ratio (a/h), gradation indexes and volume fraction of porosity on in-plane bi-directional rectangular plate (b/a=2)

a/h	Φ=0; ζ_1=1; ζ_2 =1	Φ =0.1; ζ_1=1; ζ_2 =1	Φ =0.2; ζ_1=1; ζ_2 =1	Φ =0; ζ_1=2; ζ_2 =5	Φ =0.1; ζ_1=2; ζ_2 =5	Φ =0.2;ζ_1=2; ζ_2 =5
2	1.28341	0.9364	0.53823	0.84571	0.57001	0.28529
5	2.38312	1.86496	1.2724	1.40436	0.95307	0.48656
10	2.68134	2.12537	1.50908	1.55144	1.05448	0.54061
50	2.79132	2.22182	1.59734	1.6053	1.09168	0.56053
100	2.79489	2.22495	1.60021	1.60704	1.09289	0.56118

Table 5: Effect of aspect ratio (b/a), gradation exponents and porosity on in-plane bi-directional plate with thickness ratio, a/h =10.

b/a	Φ=0; ζ_1=1; ζ_2 =1	Φ =0.1; ζ_1=1; ζ_2 =1	Φ =0.2; ζ_1=1; ζ_2 =1	Φ =0; ζ_1=2; ζ_2 =5	Φ =0.1; ζ_1=2; ζ_2	Φ =0.2;ζ_1=2; ζ_2 =5
0.5	17.64035	12.86434	7.75499	12.92137	8.59262	4.18174
1	6.43608	4.99423	3.3757	4.00744	2.74773	1.43306
1.5	3.56217	2.82248	1.99945	2.10558	1.44346	0.75601
2	2.68134	2.12537	1.50908	1.55144	1.05448	0.54061
3	2.07702	1.62917	1.1325	1.19203	0.79941	0.39619

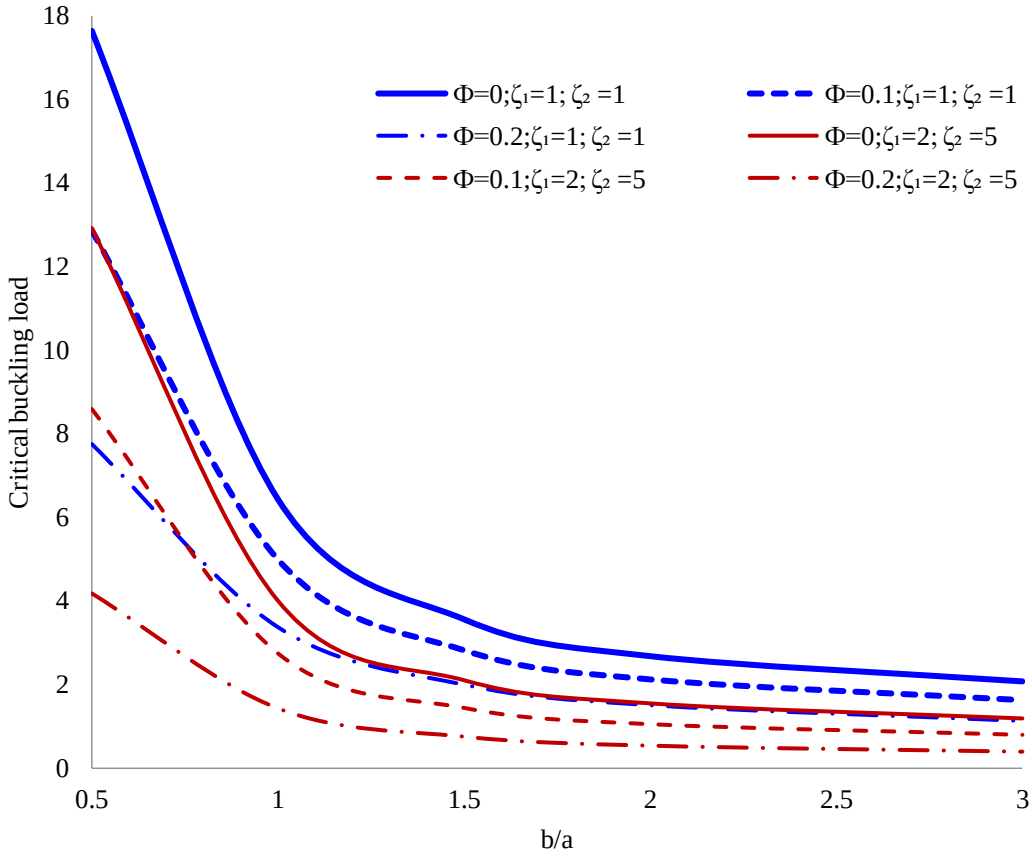

Fig 5: Effect of aspect ratio (b/a), gradation exponents and porosity on in-plane bi-directional plate with thickness ratio, a/h =10.

Table 6: Effect of thickness ratio, gradation exponents and volume fraction of porosity on in-plane bidirectional square plate

a/h	Φ=0; ζ_1=1; ζ_2 =1	Φ =0.1; ζ_1=1; ζ_2 =1	Φ =0.2; ζ_1=1; ζ_2 =1	Φ =0; ζ_1=2; ζ_2 =5	Φ =0.1; ζ_1=2; ζ_2 =5	Φ =0.2;ζ_1=2; ζ_2 =5
2	1.24519	0.89968	0.51091	0.85524	0.57439	0.28336
5	2.77574	2.14349	1.40881	1.71684	1.17291	0.60618
10	3.32647	2.62088	1.83132	2.00568	1.37671	0.7211
50	3.54702	2.81462	2.00919	2.11992	1.45773	0.76744
100	3.55434	2.82108	2.01518	2.1237	1.46042	0.76899

Table 7: Effect of aspect ratio , gradation exponents and porosity on inplane bidirectional FGP's with a/h =10

b/a	Φ=0; ζ_1=1; ζ_2 =1	Φ =0.1; ζ_1=1; ζ_2 =1	Φ =0.2; ζ_1=1; ζ_2 =1	Φ =0; ζ_1=2; ζ_2 =5	Φ =0.1; ζ_1=2; ζ_2 =5	Φ =0.2;ζ_1=2; ζ_2 =5
0.5	7.34865	5.65776	3.73799	4.507	3.05843	1.56133
1	3.32647	2.62088	1.83132	2.00568	1.37671	0.7211
1.5	2.4249	1.90621	1.32756	1.44288	0.98205	0.50322
2	2.07211	1.61593	1.10777	1.22468	0.82512	0.41262
3	1.75881	1.34622	0.89235	1.05608	0.70214	0.34057

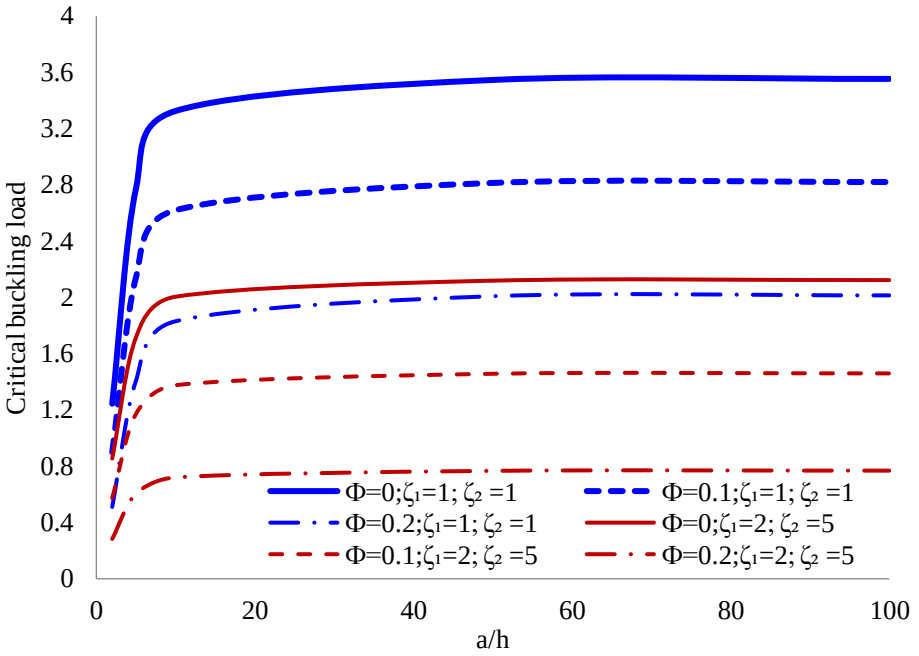

Fig 6: Effect of thickness ratio, gradation exponents and volume fraction of porosity on in-plane bidirectional square plate

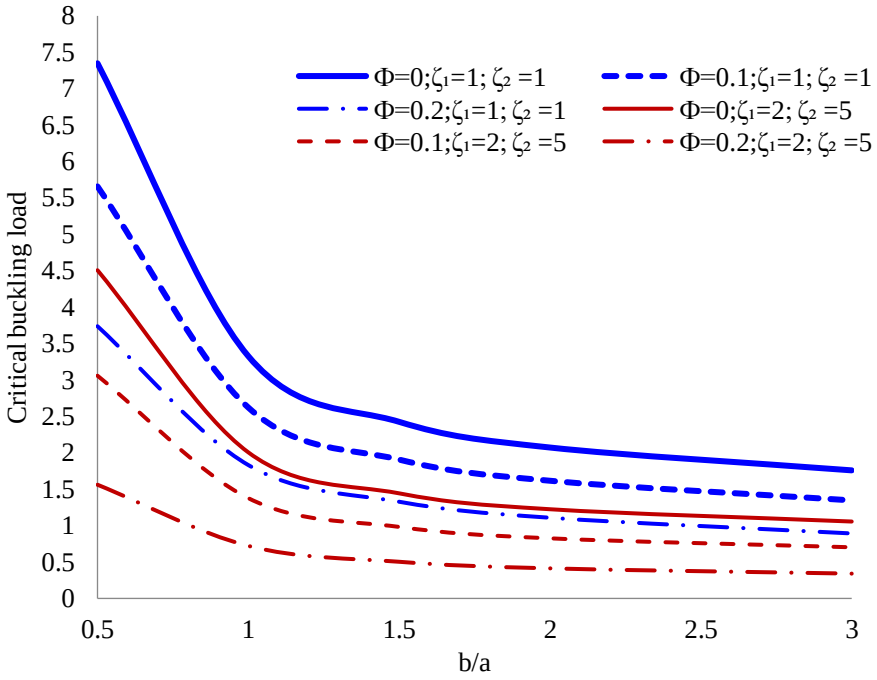

Fig 7: Effect of aspect ratio , gradation exponents and porosity on inplane bidirectional FGP's with a/h =10

The effect of b/a, ζ_1 , ζ_2, and Φ on the dimensionless critical load under biaxial compression is shown in Table 7 and Fig 7. It is observed that the critical buckling loads are larger when the plate is subjected to uniaxial compression compared to bi-axial compression. This is due to the inherent differences in load distribution and stability. In uniaxial compression, the applied force acts in a single direction, leading to a more efficient load transfer along the axis of compression, allowing the material to withstand higher loads before buckling occurs. In contrast, in biaxial compression, the applied forces act in two perpendicular directions, leading to reduced load-carrying capacity as the material experiences stress in two directions simultaneously, making it more susceptible to buckling at lower loads. Therefore, the uniaxial scenario provides a more favourable stress distribution for resisting buckling, resulting in higher critical loads.

Table 8: Influence gradation exponents and porosity on inplane bidirectional FG square plates with a/h =10

Φ	ζ_1=1; ζ_2 =1	ζ_1=1; ζ_2 =2	ζ_1=1; ζ_2 =5
0	3.32647	2.66212	2.11954
0.04	3.04988	2.39195	1.86455
0.08	2.7662	2.11577	1.60645
0.1	2.62088	1.97472	1.47588
0.12	2.47262	1.83114	1.34401
0.16	2.16427	1.53375	1.07513
0.2	1.83132	1.2149	0.79579

The effect of gradient exponents and porosity volume fraction are given in Table 8 and shown in Fig 8. From the Fig 8, it is observed that the increase of porosity volume fraction and increase of gradient index in y direction, decreases the critical buckling loads. Higher porosity reduces the material's structural integrity by creating voids that weaken its ability to support compressive loads. Additionally, increase of gradient index in the η_2-direction leads to decrease in material modulus of elasticity, causing uneven load distribution and reducing the material's overall stability and more vulnerable to structural failure under compression.

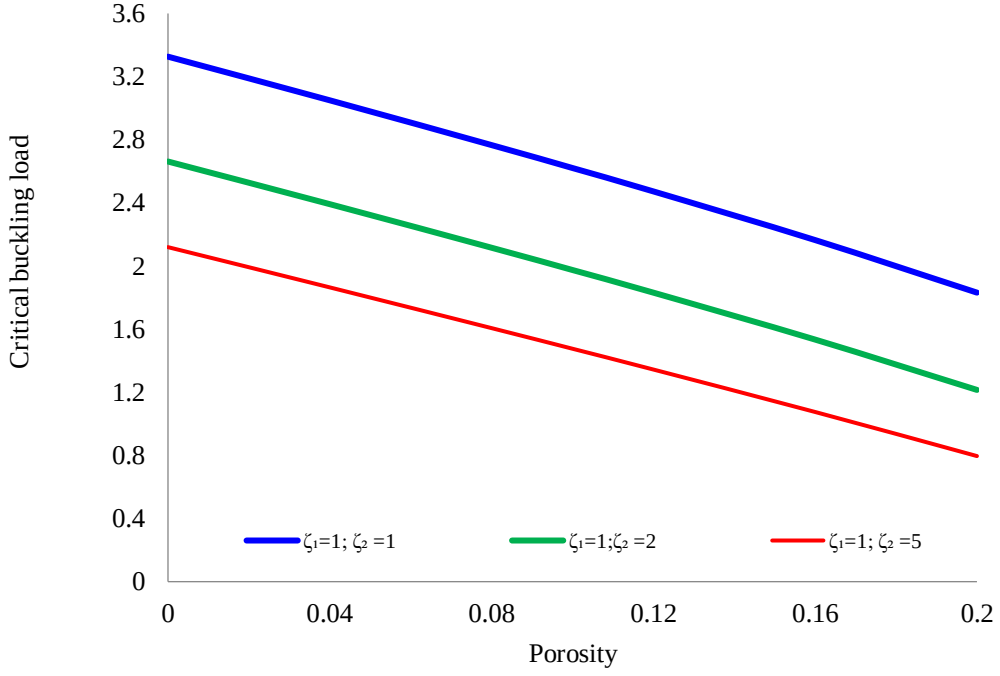

Fig.8: Influence gradation exponents and porosity on in-plane bi-directional FG square plates with side to thickness ratio (a/h) =10

4. Conclusions

In this paper, a novel approach is introduced to analyze the buckling behavior of in-plane bidirectional FGPs with a generalized higher order theory. This theory has the advantage of satisfying the nullity conditions for transverse shear stresses at the top and bottom of the plate, eliminating the need for a shear correction factor.

The properties of bidirectional porous FGPs in the in-plane direction can be modified by changing the gradation indices for both the material composition and the volume fraction of porosity. To derive the equilibrium equations governing their motion, the Lagrange equations are employed in conjunction with polynomials and additional admissible functions. These added functions are crucial for satisfying the imposed boundary conditions.

Admissible functions in this study are generated using Pascal's triangle. The research examines a range of gradation index values for both the η_1 and η_2-directions, side-to-thickness ratios, aspect ratios, and volume fractions of porosity. The critical buckling loads, calculated dimensionlessly, are then compared to findings from previous studies. Notably, the results from our generalized higher-order shear deformation theory closely align with previously published results in the literature. To gain a deeper insight into the buckling behavior of in-plane bidirectional porous FGPs, we

conducted an extensive analysis by varying the gradation indexes, side-to-thickness ratios, aspect ratios, and volume fractions of porosity.

The dimensionless critical buckling loads exhibit an increase with higher side-to-thickness ratios, while they decrease with increasing aspect ratios, gradation indexes in η_1 and η_2-directions,, and volume fraction of porosity in both uni-axial and bi-axial compression scenarios. Notably, critical buckling loads are more substantial in uniaxial compression when compared to bi-axial compression. These numerical findings serve as valuable benchmark solutions for evaluating different plate theories and for comparing them to results derived from alternative analytical and finite element methods. This study highlights the capability of the proposed theory to analyze the buckling behavior of bidirectional porous FG plates produced through the sintering process.

References

[1] M. Koizumi, FGM activities in Japan, *Composites Part B: Engineering*, Vol. 28, No. 1, pp. 1-4, 1997/01/01/, 1997.

[2] D. Chen, J. Yang, S. Kitipornchai, Free and forced vibrations of shear deformable functionally graded porous beams, *International Journal of Mechanical Sciences*, Vol. 108-109, pp. 14-22, 2016/04/01/, 2016.

[3] N. Wattanasakulpong, A. Chaikittiratana, S. Pornpeerakeat, Chebyshev collocation approach for vibration analysis of functionally graded porous beams based on third-order shear deformation theory, *Acta Mechanica Sinica*, Vol. 34, No. 6, pp. 1124-1135, 2018/12/01, 2018.

[4] S. Bathini, K. Vijaya Kumar Reddy, Flexural behavior of porous functionally graded plates using a novel higher order theory, *Journal of Computational Applied Mechanics*, Vol. 51, No. 2, pp. 361-373, 2020.

[5] S. Coskun, J. Kim, H. Toutanji, Bending, Free Vibration, and Buckling Analysis of Functionally Graded Porous Micro-Plates Using a General Third-Order Plate Theory, *Journal of Composites Science*, Vol. 3, pp. 15, 02/01, 2019.

[6] M. Mohammadi, A. R. Saidi, E. Jomehzadeh, Levy Solution for Buckling Analysis of Functionally Graded Rectangular Plates, *Applied Composite Materials*, Vol. 17, No. 2, pp. 81-93, 2010/04/01, 2010.

[7] M. Mohammadi, A. R. Saidi, E. Jomehzadeh, A novel analytical approach for the buckling analysis of moderately thick functionally graded rectangular plates with two simply-supported opposite edges, *Proceedings of the Institution of Mechanical Engineers, Part C: Journal of Mechanical Engineering Science*, Vol. 224, No. 9, pp. 1831-1841, 2010/09/01, 2010.

[8] A. Farajpour, M. Danesh, M. Mohammadi, Buckling analysis of variable thickness nanoplates using nonlocal continuum mechanics, *Physica E: Low-dimensional Systems and Nanostructures*, Vol. 44, No. 3, pp. 719-727, 2011.

[9] A. Farajpour, M. Mohammadi, A. Shahidi, M. Mahzoon, Axisymmetric buckling of the circular graphene sheets with the nonlocal continuum plate model, *Physica E: Low-dimensional Systems and Nanostructures*, Vol. 43, No. 10, pp. 1820-1825, 2011.

[10] A. Farajpour, A. Shahidi, M. Mohammadi, M. Mahzoon, Buckling of orthotropic micro/nanoscale plates under linearly varying in-plane load via nonlocal continuum mechanics, *Composite Structures*, Vol. 94, No. 5, pp. 1605-1615, 2012.

[11] M. Mohammadi, A. Farajpour, A. Moradi, M. Ghayour, Shear buckling of orthotropic rectangular graphene sheet embedded in an elastic medium in thermal environment, *Composites Part B: Engineering*, Vol. 56, pp. 629-637, 2014.

[12] M. Abdollahi, A. R. Saidi, M. Mohammadi, Buckling analysis of thick functionally graded piezoelectric plates based on the higher-order shear and normal deformable theory, *Acta Mechanica*, Vol. 226, No. 8, pp. 2497-2510, 2015/08/01, 2015.

[13] M. Mohammadi, M. Fooladi Mahani, An analytical solution for buckling analysis of size-dependent rectangular micro-plates according to the modified strain gradient and couple stress theories, *Acta Mechanica*, Vol. 226, No. 10, pp. 3477-3493, 2015/10/01, 2015.

[14] A. Farajpour, M. H. Yazdi, A. Rastgoo, M. Mohammadi, A higher-order nonlocal strain gradient plate model for buckling of orthotropic nanoplates in thermal environment, *Acta Mechanica*, Vol. 227, pp. 1849-1867, 2016.

[15] A. Farajpour, A. Rastgoo, M. Mohammadi, Vibration, buckling and smart control of microtubules using piezoelectric nanoshells under electric voltage in thermal environment, *Physica B: Condensed Matter*, Vol. 509, pp. 100-114, 2017.

[16] B. S. Reddy, J. S. Kumar, C. E. Reddy, K. V. K. Reddy, Buckling Analysis of Functionally Graded Material Plates Using Higher Order Shear Deformation Theory, *Journal of Composites*, Vol. 2013, pp. 808764, 2013/12/23, 2013.

[17] B. S. Reddy, J. S. Kumar, C. E. Reddy, K. V. K. Reddy, Buckling Analysis of Functionally Graded Plates Using Higher Order Shear Deformation Theory with Thickness Stretching Effect, *International Journal of Applied Science and Engineering*, Vol. 13, No. 1, pp. 19-35, 2015/03/01, 2015.

[18] J. Kim, K. K. Żur, J. N. Reddy, Bending, free vibration, and buckling of modified couples stress-based functionally graded porous micro-plates, *Composite Structures*, Vol. 209, pp. 879-888, 2019/02/01/, 2019.

[19] P. Van Vinh, N. Van Chinh, A. Tounsi, Static bending and buckling analysis of bi-directional functionally graded porous plates using an improved first-order shear deformation theory and FEM, *European Journal of Mechanics - A/Solids*, Vol. 96, pp. 104743, 2022/11/01/, 2022.

[20] D. Chen, J. Yang, S. Kitipornchai, Buckling and bending analyses of a novel functionally graded porous plate using Chebyshev-Ritz method, *Archives of Civil and Mechanical Engineering*, Vol. 19, No. 1, pp. 157-170, 2019/03/01, 2019.

[21] M. Nemat-Alla, Reduction of thermal stresses by developing two-dimensional functionally graded materials, *International Journal of Solids and Structures*, Vol. 40, No. 26, pp. 7339-7356, 2003/12/01/, 2003.

[22] P. V. Vinh, Analysis of bi-directional functionally graded sandwich plates via higher-order shear deformation theory and finite element method, *Journal of Sandwich Structures & Materials*, Vol. 24, No. 2, pp. 860-899, 2022/02/01, 2021.

[23] M. Nemat-Alla, Reduction of thermal stresses by composition optimization of two-dimensional functionally graded materials, *Acta Mechanica*, Vol. 208, No. 3, pp. 147-161, 2009/12/01, 2009.

[24] M. Asgari, M. Akhlaghi, Natural frequency analysis of 2D-FGM thick hollow cylinder based on three-dimensional elasticity equations, *European Journal of Mechanics - A/Solids*, Vol. 30, No. 2, pp. 72-81, 2011/03/01/, 2011.

[25] M. J. Ebrahimi, M. M. Najafizadeh, Free vibration analysis of two-dimensional functionally graded cylindrical shells, *Applied Mathematical Modelling*, Vol. 38, No. 1, pp. 308-324, 2014/01/01/, 2014.

[26] L. Li, X. Li, Y. Hu, Nonlinear bending of a two-dimensionally functionally graded beam, *Composite Structures*, Vol. 184, pp. 1049-1061, 2018/01/15/, 2018.

[27] M. Şimşek, Bi-directional functionally graded materials (BDFGMs) for free and forced vibration of Timoshenko beams with various boundary conditions, *Composite Structures*, Vol. 133, pp. 968-978, 2015/12/01/, 2015.

[28] Y. Tang, Q. Ding, Nonlinear vibration analysis of a bi-directional functionally graded beam under hygro-thermal loads, *Composite Structures*, Vol. 225, pp. 111076, 2019/10/01/, 2019.

[29] M. Şimşek, Buckling of Timoshenko beams composed of two-dimensional functionally graded material (2D-FGM) having different boundary conditions, *Composite Structures*, Vol. 149, pp. 304-314, 2016/08/01/, 2016.

[30] M. Z. Nejad, A. Hadi, A. Rastgoo, Buckling analysis of arbitrary two-directional functionally graded Euler–Bernoulli nano-beams based on nonlocal elasticity theory, *International Journal of Engineering Science*, Vol. 103, pp. 1-10, 2016/06/01/, 2016.

[31] A. Karamanlı, Bending behaviour of two directional functionally graded sandwich beams by using a quasi-3d shear deformation theory, *Composite Structures*, Vol. 174, pp. 70-86, 2017/08/15/, 2017.

[32] M. Lezgy-Nazargah, Fully coupled thermo-mechanical analysis of bi-directional FGM beams using NURBS isogeometric finite element approach, *Aerospace Science and Technology*, Vol. 45, pp. 154-164, 2015/09/01/, 2015.

[33] M. K. Apalak, M. D. Demirbas, Thermal stress analysis of in-plane two-directional functionally graded plates subjected to in-plane edge heat fluxes, *Proceedings of the Institution of Mechanical Engineers, Part L: Journal of Materials: Design and Applications*, Vol. 232, No. 8, pp. 693-716, 2018/08/01, 2016.

[34] T. Van Do, D. K. Nguyen, N. D. Duc, D. H. Doan, T. Q. Bui, Analysis of bi-directional functionally graded plates by FEM and a new third-order shear deformation plate theory, *Thin-Walled Structures*, Vol. 119, pp. 687-699, 2017/10/01/, 2017.

[35] Q. X. Lieu, S. Lee, J. Kang, J. Lee, Bending and free vibration analyses of in-plane bi-directional functionally graded plates with variable thickness using isogeometric analysis, *Composite Structures*, Vol. 192, pp. 434-451, 2018/05/15/, 2018.

[36] Q. X. Lieu, D. Lee, J. Kang, J. Lee, NURBS-based modeling and analysis for free vibration and buckling problems of in-plane bi-directional functionally graded plates, *Mechanics of Advanced Materials and Structures*, Vol. 26, No. 12, pp. 1064-1080, 2019/06/18, 2019.

[37] M. Chen, G. Jin, X. Ma, Y. Zhang, T. Ye, Z. Liu, Vibration analysis for sector cylindrical shells with bi-directional functionally graded materials and elastically restrained edges, *Composites Part B: Engineering*, Vol. 153, pp. 346-363, 2018/11/15/, 2018.

[38] M. Esmaeilzadeh, M. Kadkhodayan, Dynamic analysis of stiffened bi-directional functionally graded plates with porosities under a moving load by dynamic relaxation method with kinetic damping, *Aerospace Science and Technology*, Vol. 93, pp. 105333, 2019/10/01/, 2019.

[39] A. Barati, A. Hadi, M. Z. Nejad, R. Noroozi, On vibration of bi-directional functionally graded nanobeams under magnetic field, *Mechanics Based Design of Structures and Machines*, Vol. 50, No. 2, pp. 468-485, 2022/02/01, 2022.

[40] X. Chen, Y. Lu, Z. Wu, Y. Shao, X. Xue, Y. Wu, Free vibration of in-plane bi-directional functionally graded materials rectangular plates with geometric imperfections and general elastic restraints, *Aerospace Science and Technology*, Vol. 132, pp. 108045, 2023/01/01/, 2023.

[41] J. Zhu, Z. Lai, Z. Yin, J. Jeon, S. Lee, Fabrication of ZrO2–NiCr functionally graded material by powder metallurgy, *Materials Chemistry and Physics*, Vol. 68, No. 1, pp. 130-135, 2001/02/15/, 2001.

[42] S. R. Bathini, V. K. R. K, C. A. B, Free vibration behavior of bi-directional functionally graded plates with porosities using a refined first order shear deformation theory, *Journal of Computational Applied Mechanics*, Vol. 51, No. 2, pp. 374-388, 2020.

[43] R. Kolahchi, M. Safari, M. Esmailpour, Dynamic stability analysis of temperature-dependent functionally graded CNT-reinforced visco-plates resting on orthotropic elastomeric medium, *Composite Structures*, Vol. 150, pp. 255-265, 2016.

[44] R. Kolahchi, S.-P. Zhu, B. Keshtegar, N.-T. Trung, Dynamic buckling optimization of laminated aircraft conical shells with hybrid nanocomposite martial, *Aerospace Science and Technology*, Vol. 98, pp. 105656, 2020.

[45] B. Keshtegar, A. Farrokhian, R. Kolahchi, N.-T. Trung, Dynamic stability response of truncated nanocomposite conical shell with magnetostrictive face sheets utilizing higher order theory of sandwich panels, *European Journal of Mechanics-A/Solids*, Vol. 82, pp. 104010, 2020.

[46] B. Keshtegar, M. Motezaker, R. Kolahchi, N.-T. Trung, Wave propagation and vibration responses in porous smart nanocomposite sandwich beam resting on Kerr foundation considering structural damping, *Thin-Walled Structures*, Vol. 154, pp. 106820, 2020.

[47] H. Golabchi, R. Kolahchi, M. R. Bidgoli, Vibration and instability analysis of pipes reinforced by SiO2 nanoparticles considering agglomeration effects, *Computers and Concrete, An International Journal*, Vol. 21, No. 4, pp. 431-440, 2018.

[48] M. H. Hajmohammad, M. Maleki, R. Kolahchi, Seismic response of underwater concrete pipes conveying fluid covered with nano-fiber reinforced polymer layer, *Soil Dynamics and Earthquake Engineering*, Vol. 110, pp. 18-27, 2018.

[49] M. S. H. Al-Furjan, A. Farrokhian, B. Keshtegar, R. Kolahchi, N.-T. Trung, Dynamic stability control of viscoelastic nanocomposite piezoelectric sandwich beams resting on Kerr foundation based on exponential piezoelasticity theory, *European Journal of Mechanics - A/Solids*, Vol. 86, pp. 104169, 2021/03/01/, 2021.

[50] M. Al-Furjan, A. Farrokhian, S. Mahmoud, R. Kolahchi, Dynamic deflection and contact force histories of graphene platelets reinforced conical shell integrated with magnetostrictive layers subjected to low-velocity impact, *Thin-Walled Structures*, Vol. 163, pp. 107706, 2021.

[51] M. H. Hajmohammad, A. H. Nouri, M. S. Zarei, R. Kolahchi, A new numerical approach and visco-refined zigzag theory for blast analysis of auxetic honeycomb plates integrated by multiphase nanocomposite facesheets in hygrothermal environment, *Engineering with Computers*, Vol. 35, pp. 1141-1157, 2019.

[52] R. Kolahchi, F. Kolahdouzan, A numerical method for magneto-hygro-thermal dynamic stability analysis of defective quadrilateral graphene sheets using higher order nonlocal strain gradient theory with different movable boundary conditions, *Applied Mathematical Modelling*, Vol. 91, pp. 458-475, 2021.

[53] M. H. Hajmohammad, M. B. Azizkhani, R. Kolahchi, Multiphase nanocomposite viscoelastic laminated conical shells subjected to magneto-hygrothermal loads: Dynamic buckling analysis, *International Journal of Mechanical Sciences*, Vol. 137, pp. 205-213, 2018.

[54] M. Al-Furjan, A. Farrokhian, B. Keshtegar, R. Kolahchi, N.-T. Trung, Higher order nonlocal viscoelastic strain gradient theory for dynamic buckling analysis of carbon nanocones, *Aerospace Science and Technology*, Vol. 107, pp. 106259, 2020.

[55] H.-T. Thai, D.-H. Choi, An efficient and simple refined theory for buckling analysis of functionally graded plates, *Applied Mathematical Modelling*, Vol. 36, No. 3, pp. 1008-1022, 2012/03/01/, 2012.

[56] A. M. Zenkour, Generalized shear deformation theory for bending analysis of functionally graded plates, *Applied Mathematical Modelling*, Vol. 30, No. 1, pp. 67-84, 2006/01/01/, 2006.

[57] H.-T. Thai, S.-E. Kim, Closed-form solution for buckling analysis of thick functionally graded plates on elastic foundation, *International Journal of Mechanical Sciences*, Vol. 75, pp. 34-44, 2013/10/01/, 2013.

[58] X. Zhao, Y. Y. Lee, K. M. Liew, Mechanical and thermal buckling analysis of functionally graded plates, *Composite Structures*, Vol. 90, No. 2, pp. 161-171, 2009/09/01/, 2009.